Hindawi
Advances in Materials Science and Engineering
Volume 2018, Article ID 3019158, 9 pages
https://doi.org/10.1155/2018/3019158

Research Article

Using X-Ray CT Scanning to Study the Failure Mechanism of Concrete under Static and Dynamic Loadings

Guangyu Lei,[1] **Jichang Han**,[1] **and Faning Dang**[2]

[1]*Shaanxi Provincial Land Engineering Construction Group Co., Ltd., Xi'an 710075, China*
[2]*Institute of Geotechnical Engineering, Xi'an University of Technology, Xi'an 710048, China*

Correspondence should be addressed to Guangyu Lei; leiyugogo@163.com

Received 14 May 2018; Accepted 26 October 2018; Published 14 November 2018

Academic Editor: Barbara Liguori

X-ray images can be used to nondestructively monitor the initiation, extension, and combination of cracks in concrete. In this study, real-time X-ray computed tomography (CT) scanning of concrete specimens under static and dynamic loadings was done. The CT images showed the growth, propagation, and penetration of the cracks and showed the ultimate failure of the concrete samples. Analysis of the CT images and CT numbers showed that the failure followed the structure's areas of weakness under the static load, but for dynamic loading, the cracks formed very rapidly along straight lines through the aggregate.

1. Introduction

Because of concrete's plasticity, compressive capacity, and durability, it is widely used in construction. Large concrete structures are impacted by static loads that change slowly and dynamic loads that change rapidly. The changes in concrete, such as failure modes, under dynamic loads are very different from those under static loads. There has been a lot of fruitful research on the dynamic characteristics of concrete [1–4], but there have been few studies of the process of mesoscopic damage using CT scan technology [5–8]. Raphael [9] found that the dynamic strength of concrete is about 30% higher than its static strength and that the dynamic tensile strength is about 10% higher than that of the dynamic compressive strength. Harris et al. [10] studied the dynamic characteristics of bulk concrete sampled from dam cores. The results obtained were different from those obtained by Raphael, and the resulting dynamic strength enhancement factor was found to be significantly less than Raphael's value. Cadoni et al. [11] studied concrete behavior with direct tension tests at high strain rates and found a significant increase in tensile strength, failure strain, elastic modulus, and fracture energy as the strain rates increased. Elmer et al. [12] proposed a new mechanism for the increase in dynamic strength over static strength, focusing on the failure mechanism known as shear faulting. Chen and Ding [13] used X-ray computed tomography with real-time internal CT images of concrete to observe the mesoscopic failure process of concrete under uniaxial compression. Their images showed crack initiation, crack expansion, and crack coalescence. By using the knowledge of the set theory, Dang et al. [14] studied where cracks appeared and the criteria for damage and established the partition space for concrete constitutive relationships and the concrete damage constitutive theory. Dang et al. [14] also described the concepts of safety zone, damaging zone, and damaged zone.

An increase in the strength of concrete when dynamically loaded has been noted in the literature since the early twentieth century, and despite having been observed in a variety of tests, the explanations or mechanisms leading to this increase have not been satisfactorily established. A variety of factors, including aspects of the test setup and specimen preparation, have been shown to influence the outcome of the tests. More recently, CT tests of concrete have been used to analyze and predict the failure mechanism of concrete under both static and dynamic loadings.

In our work, we used CT images of the damage process of concrete under static and dynamic loadings. We analyzed concrete CT images and CT numbers for many scanning planes to determine the relationships between concrete

strength and different loadings, and we used this information to analyze the various failure modes. We discovered that, on the mesoscopic level, the dynamic strength of concrete is greater than its static strength, and we have provided reference values that can be used for further study of concrete materials.

2. Materials and Methods

2.1. CT Test Loading System. Concrete CT refers to nondestructively observing and studying the internal structure of concrete samples using X-ray computed tomography (CT). We did CT scans on layers of concrete that were 0.3 mm thick. The observed cracks can be called CT scale cracks. The benefit of using CT technology is that one can observe the whole process of the evolution of cracks from their formation through their growth for concrete under static and dynamic loadings. The minimum width of a recognizable crack is 0.01 mm. Our team successfully developed a dynamic loading device for CT scanning using a medical CT machine, and as far as we know, it is the first of its type anywhere. It is mainly composed of three parts: loading host, actuator, and digital measuring controller. The weight of the loading host of the instrument is less than 45 kg. The axial tension and compression maximum output is 100 kN, and the frequency is 5 Hz. The digital controller (EDC) uses the digital controller produced by Germany DOLI Company. It can be applied to studying the dynamic tensile and compressive strengths of rock and concrete. Figure 1 shows the structure of the material testing machine. The instrument has a variety of advantages, including a low mass structure that is easy to move, easy to install, has smooth operation, and allows for different loading modes. Figure 2 shows the equipment for the CT tests.

2.2. CT Test Design

2.2.1. Test Materials. The concrete cylinder specimens used had a diameter of 60 mm and a height of 120 mm and were aged for ten months. The aggregate had one gradation. The ratio of the materials used to make the concrete was the same as that of the concrete used to make the DaGang mountain arch dam. The mixture ratio of water/cement/fly ash/sand/stone is 86/134/57/534/1607. Sand selects natural sand in the natural material yard of DaGang mountain hydropower station. The aggregate is monzonitic granite. The cement is Emei Mountain brand middle heat 42.5 cement. Fly ash is Guang'an brand grade 1 fly ash.

2.2.2. Loading Project. First, we set the loading rate based on the average strength of the processed specimens. Initially, we used the load control to add enough load to get close to the material's strength value, and after that, the displacement control was used to control the specimen failure and crack development.

2.2.3. Test Procedure. The preparatory work included sampling, centering, bonding, and installation. This was followed by connecting the instrument, putting the specimen in the CT machine, and beginning the scans. Each specimen was first scanned before loading, followed by increasing the load close to the material's strength at a rate that was the same for all scans. Periodic scans were done during the initial load control phase. This was followed by increasing the load with the displacement control. The rate of increasing load using the displacement control was set to keep the slope of the stress-strain curve the same for each stage of the process. To find this rate, we determined the displacement amplitude based on the rate for the load control stage that was consistent with the slope of the stress-strain curve. The scan time for the displacement control loading was based on two principles. First, when the loading value was close to the material strength, we paused the scanning. Second, when the stress-strain curve began its downward trend, we kept the displacement unchanged and continued the scanning. We stopped scanning when the specimen broke.

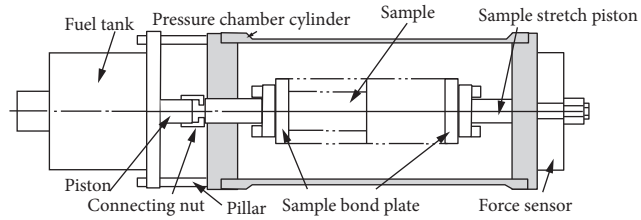

Figure 1: The structural diagram of the loading equipment for CT scanning.

3. Results and Discussion

3.1. Analysis Method. Because concrete CT images can display internal mesoscopic cracks in concrete, they can be used in research that involves the analysis of concrete. Concrete CT grayscale images can be constructed with different degrees of gray from black to white pixels arranged in a matrix. The use of concrete CT images is only limited by the ability of the naked eye to see the real crack propagation from the concrete CT images. The concrete CT images can be analyzed based on the different densities that are reflected by CT numbers, which describe the degree to which X-rays can pass through a sample.

An enhanced image of the cracks in concrete can be created by subtracting the CT numbers at the same positions in concrete CT images for the same cross section at different stress stages. Cracks are indicated where there are significant differences between the CT numbers, and where there are no cracks, there will be no significant difference in the CT numbers. Crack initiation and extension are indicated when the CT number decreases significantly. The crack indicated by the CT number differences can be linear or circular. Compared with the original CT images, the new image shows the cracks more clearly. Figure 3 shows two images that were compared and an enhanced image created by CT number comparison.

Density levels can be highlighted with color, with different colors associated with different density levels. These

(a) (b)

Figure 2: The CT machine and loading instrument. (a) CT output display. (b) CT machine and power loading instrument.

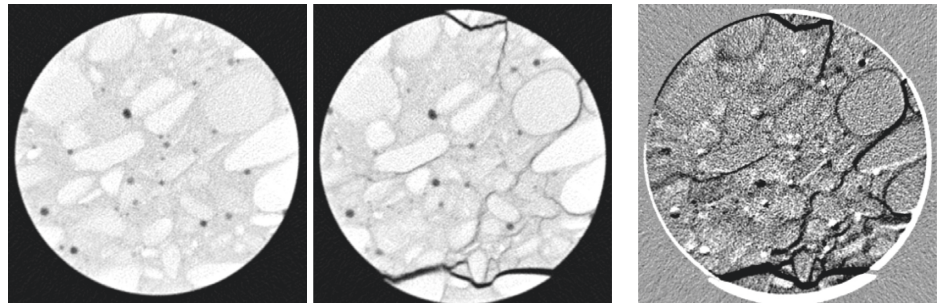

(a) (b)

Figure 3: (a) The CT images for the same cross section at different stress stages; (b) the image created from the differences in CT number at each position of (a), which shows the cracks more clearly.

isodensity color images of CT scans of concrete sections can more clearly show changes within the concrete. Figure 4 shows images for different stress times.

Analysis based on CT numbers makes the study of the evolution of mesoscopic damage of rock and concrete possible. CT numbers reflect the variation of the density of the material, and this variation provides a quantitative analytical method for assessing damage.

3.2. Static Loading Test Results

3.2.1. Static Pressure Test. One specimen (CON066) was loaded by static pressure. Figure 5 shows its load displacement curve. The loading begins after point A on the graph, and points A and B represent the first scans for the load control stage. The loading rate was 0.5 kN/s, and when the load got to 30 kN, the second stage begins as the displacement control starts with a rate of 0.005 mm/s. When the load reaches 75 kN at point C, the third scan was performed. At this stage, it can be seen from Figure 5 that the load decreases slightly. This is because the specimen itself has residual stresses and because of other factors, including the relaxation of the test glue and relaxation of the pressure chamber. At point D, where there is some decline in the load, the loading was stopped and a fourth scan was done. The loading was started again, and the load rose to point E. When the load began to drop, the loading was stopped and fifth scan was done. When the specimen was completely destroyed, a sixth scan was done at the point F. Point E represents the maximum load that the specimen can withstand without destruction. The failure strength of the specimen under static pressure was found to be 33 MPa.

Figure 6 shows images of the six CT scan sections, and Figure 7 shows the graphs of CT numbers for the six stress stages of the experiment. Although the specimen changed on the microscopic level, there were no significant changes in the CT number for the first five stages for each of the sections. The increase in the CT number at the second stage is due to compaction, but because the elastic modulus of the concrete is large and the deformation is small, the amount of CT number change in this compaction phase is small. There was a slight decrease in the CT number for stress stages 3, 4, and 5, indicating decreasing density, suggesting that the specimen is in an expansion phase that is due to the beginning of crack formation. The sixth scan image shows multiple cracks, leading to significant expansion, and the sharp decrease in the CT number reflects a rapid decrease in density and significant damage to the specimen. The crack distribution is symmetrical and parallel to the loading direction.

3.2.2. Static Tension Test. One specimen (CON042) was loaded by static tension. Figure 8 shows its load displacement curve. The rate of loading was 0.02 kN/s up to 2 kN/s when the displacement was 0.05 mm. The rate of

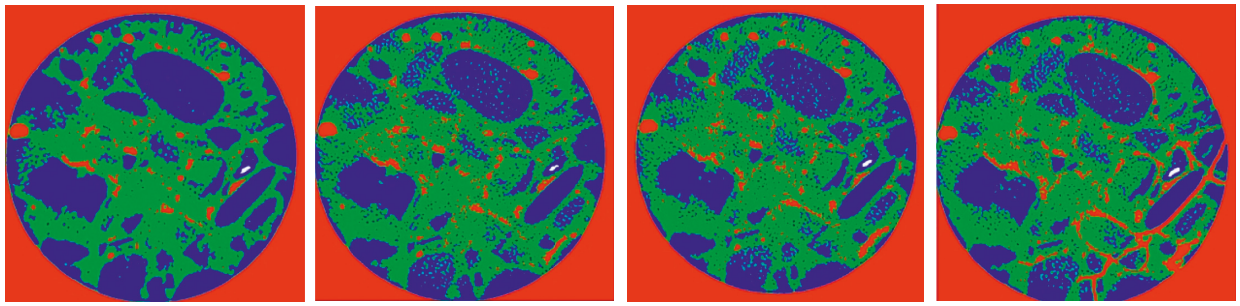

Figure 4: Isodensity segmentation images for different stress stages.

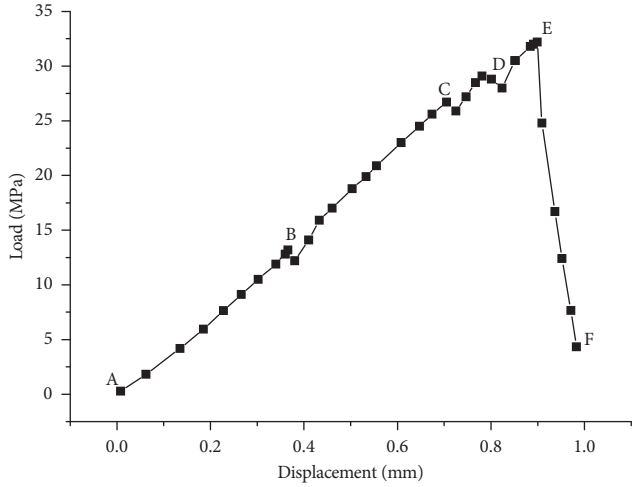

Figure 5: A load-displacement curve for static pressure on specimen CON066.

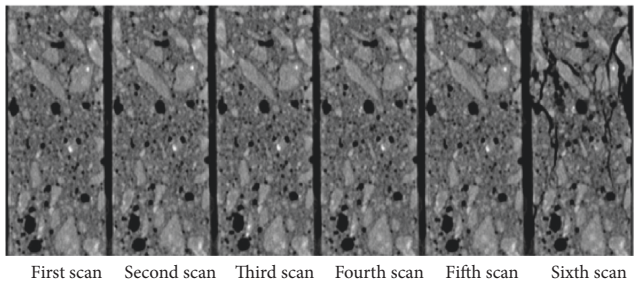

Figure 6: Sectional CT scan images for static loading for specimen CON066.

displacement was 0.002 mm/s, and the specimen fractured when the displacement was 0.17 mm. We did six scans, indicated on the graph in Figure 8 by A–F.

The load-displacement curve shows that, under a static tension loading, increasing load leads to increasing displacement in a roughly linear way. After scans B, C, and D, the load and displacement stayed essentially the same as between scans A and B. When the loading increased after scan E, the specimen fractured and the load fell rapidly. This shows that, when the concrete is subjected to tensile force, its failure is due to a brittle fracture. The curve shows that,

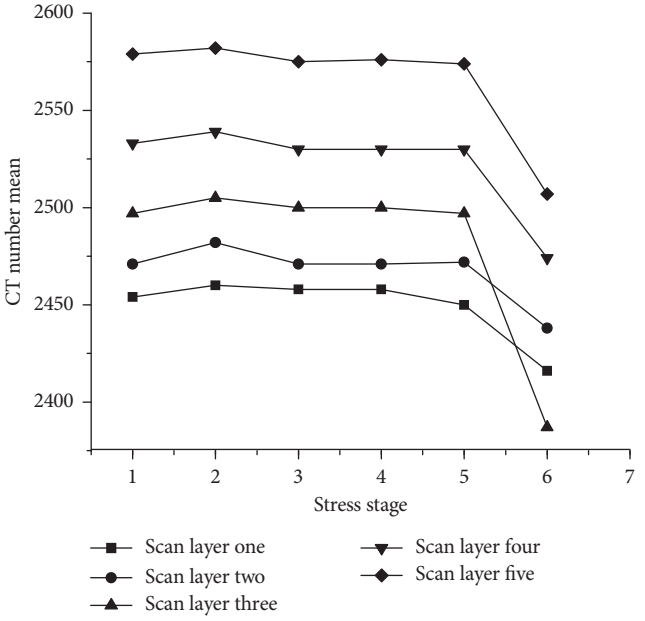

Figure 7: The curves of CT numbers for the six stress stages for specimen CON066.

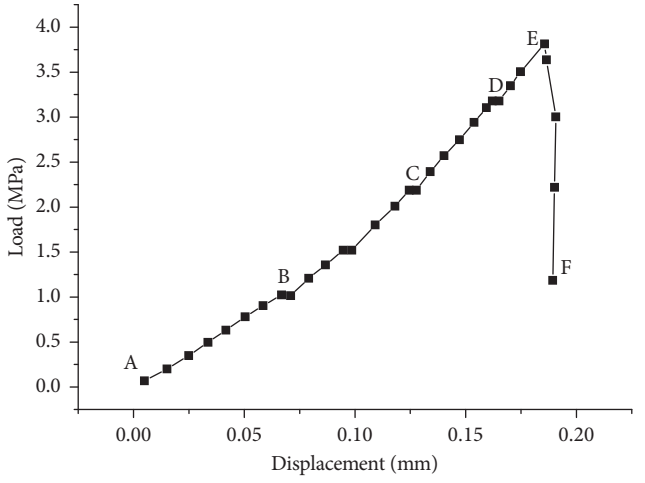

Figure 8: The load-displacement curve for specimen CON042 under static tension loading.

under the action of a static tension loading, the strength of the specimen is 3.8 MPa, which is about 1/10 of the static pressure strength.

Figure 9 shows the sectional CT scan images for static tension loading. Before destruction of the specimen, the scans look nearly the same, and there are no obvious cracks. When scanned for the last time, the specimen shows damage. Throughout the specimen, you can clearly see transverse cracks that are perpendicular to the loading direction. Figure 10 shows the curves of CT numbers at different phases of stress. For the initial stages of loading for scan layer 2, unlike the trends for CT numbers for all of the layers of the compressed specimen CON066, the mean CT numbers decrease more quickly. This suggests that the density of the concrete for this layer decreases rapidly and that microcracks and voids inside the specimen are more deformed under tensile load. Unlike the CT numbers for the compression test, the layers of the specimen subjected to tension loading did not have a compaction phase and went directly to the expansion stage. With continuous loading, the average CT numbers of the layers changed little, and a large number of microcracks in each layer expanded and penetrated each other. The mean CT number decreases drastically between the fifth and sixth scans, indicating that the density of each point in the concrete decreases rapidly due to macroscopic cracks forming and specimen failure.

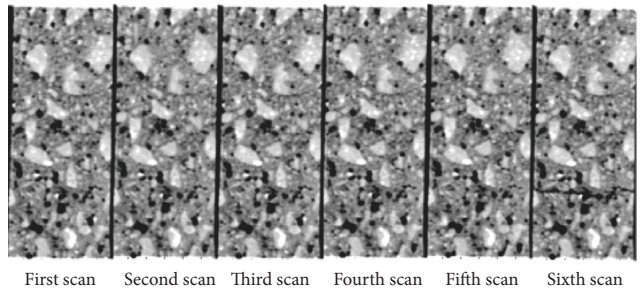

Figure 9: Sectional CT scan images for static tension loading for specimen CON042.

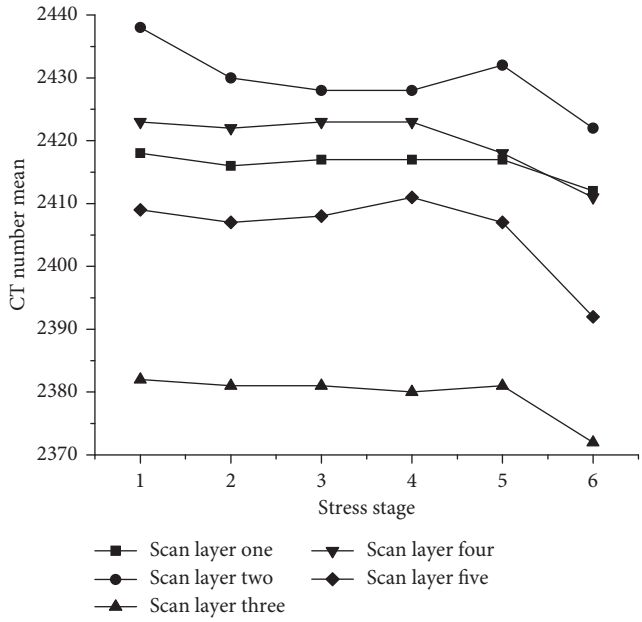

Figure 10: The curves of CT numbers for the six stress stages for specimen CON042.

3.3. Dynamic Loading Test Results

3.3.1. Dynamic Pressure Test. One specimen (CON073) was loaded by dynamic pressure. For the dynamic pressure test, the load frequency was 1 Hz, and the loading cycle was 3 s. Figure 11 shows the load displacement curve of the specimen tested. Initially, the load increased from 0.1 kN to 30 kN, at which point the displacement control took over with the increase of 0.005 mm. When the displacement reached 0.1 mm, it automatically stopped every 0.05 mm. When the displacement reached 0.7 mm, the specimen broke. There were four scans. The strength of the specimen was found to be 37 MPa.

Figure 12 shows the original CT image and the enhanced images created from CT number differences of the specimen under dynamic pressure loading. The first image in Figure 12 is the original image. You can see the location of the specimen's aggregate. The second and third images are the images created from CT number differences for the initial loading stage. There is essentially no difference between the images, indicating that microcracks have not yet formed. As the loading continues, the fourth image shows that cracks are forming and damage has begun. A comparison of this information with the static loading failure process shows that under the action of dynamic loading, the cracks develop more rapidly, the damage process comes more quickly, and the damage area is larger.

It is not clear from Figure 12(b) that there were any changes in the specimen before the failure is observed, but the graph in Figure 13 of CT numbers at various stages in the dynamic pressure loading of a concrete specimen indicates

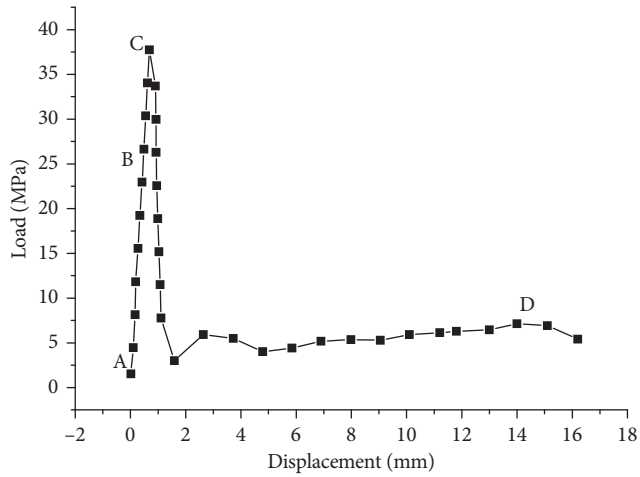

Figure 11: The load-displacement curve for specimen CON073 under dynamic pressure loading.

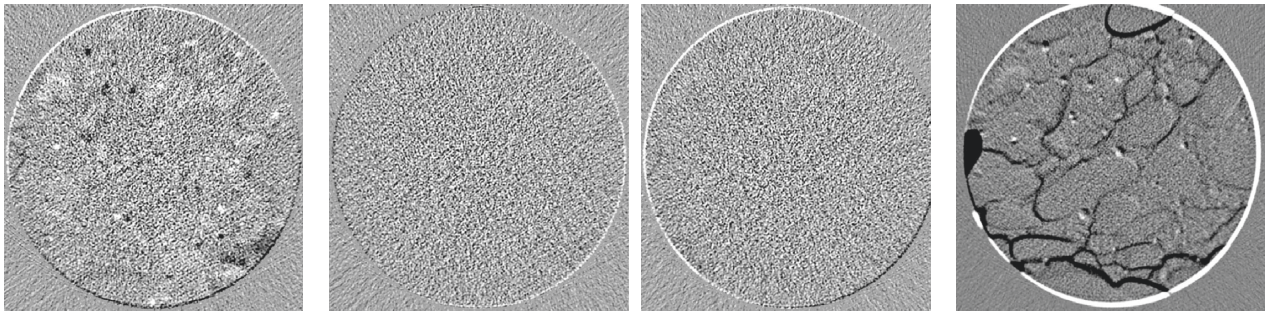

Figure 12: (a) The initial CT image. (b) The images created from CT number differences during the initial dynamic pressure loading. (c) The image created from CT number differences for the specimen after cracks began to form during dynamic pressure loading.

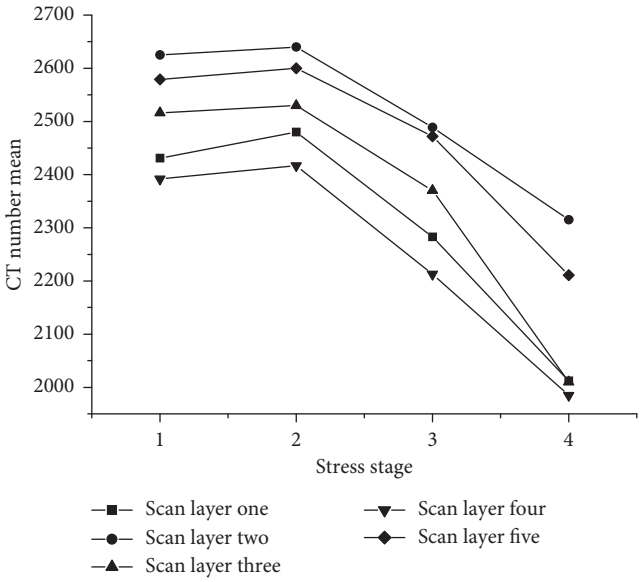

Figure 13: The curves of CT numbers for the four stress stages for specimen CON073.

Figure 14: The failure of two specimens subjected to dynamic pressure loading.

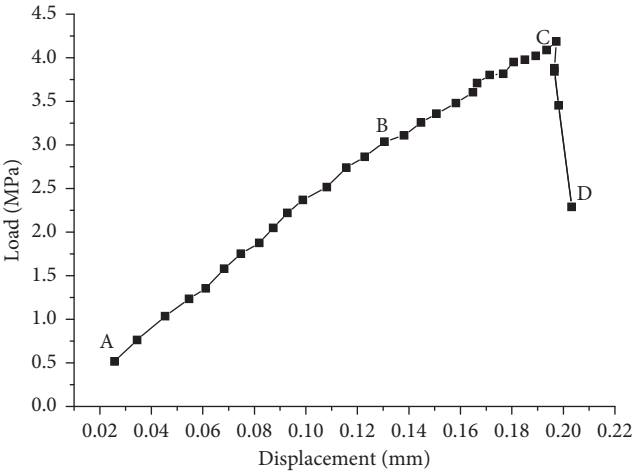

Figure 15: The load-displacement curve for specimen CON080 under dynamic tension loading.

that there were significant changes in material density. The changes of the CT number show that the density increased at first due to compaction, and then the density decreased due to the formation of cracks before the final destruction process. The study of the morphology of the concrete damage under the dynamic pressure loading shows that fractures occurred throughout the aggregate. When the specimen failed, many cracks formed at the same time and the damage happened very quickly throughout the concrete (Figure 14). The development of the cracks followed the fastest energy path under dynamic pressure loading, which is different from the development of cracks along the structural surface under static pressure loading.

3.3.2. Dynamic Tension Test. One specimen (CON080) was loaded by dynamic tension. For the dynamic tension test, the load frequency was 1 Hz and the load cycle was 3 s. Figure 15 shows the load vs. displacement graph for this process. At first, the load control was used to increase the load by 0.1 kN for each cycle. When the load reached 8 kN, we switched to the displacement control. When the tensile load was 10.8 kN, the specimen broke. Figure 15 shows that the dynamic tensile strength is 4.1 MPa.

Figure 16 shows isodensity segmentation maps created from CT numbers for a specimen under different dynamic tensile loadings. The mortar is green, aggregate is white, and holes are black. The first three scans show that the specimen did not change significantly under the initial loading. When the specimen failed, we see black lines representing cracks

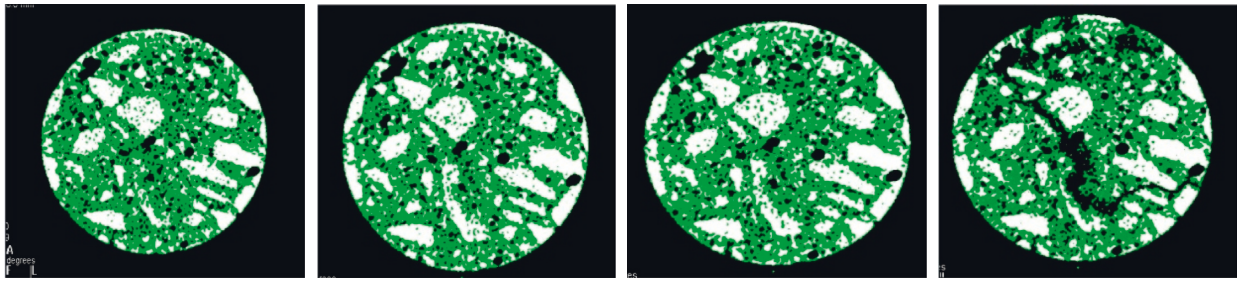

Figure 16: The CT isodensity segmentation maps under different dynamic tensile loading.

running through the test piece. This shows that when the concrete specimen is subjected to dynamic tensile loading, the microcracks formed quickly and merged to form a main crack through the specimen.

It is difficult to observe the changes in the specimen before the failure from the CT isodensity segmentation maps, but the graph in Figure 17 of CT numbers at different loading stages shows that there are changes in material density under increasing dynamic tension load. A total of four scans were performed on the specimen. As the dynamic tension load increased, the CT number decreased slightly, showing that the density of the specimen decreased. There was no compression stage for the initial loading, which is different from the dynamic pressure load. As the load continued to increase, the CT number continued to decrease, indicating that microcracks gradually form, decreasing the density. After the fourth scan, it was found that the microcracks penetrated throughout the specimen, resulting in macroscopic cracks. At this point, the decrease in the CT number was at its maximum, indicating that at the final step in the loading, the specimen was on the verge of destruction. Figure 18 shows that, under the action of dynamic tensile loading, the failure is caused by a main crack penetrating the specimen. The fracture is abrupt, and the fracture passes through the aggregate. The fracture surface is flat and horizontal, showing an obvious brittle failure.

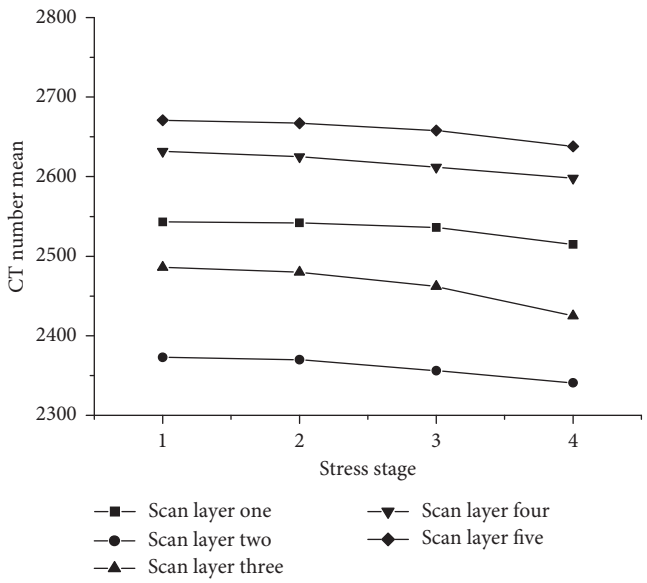

Figure 17: The curves of CT numbers for the four stress stages for specimen CON080.

3.4. Comparative Analysis of Static and Dynamic Load Failure. The damage area and failure energy of a specimen under static pressure and static tension were calculated, and the results are shown in Table 1.

Table 1 shows that concrete compressive strength for static pressure loading is ten times the strength for static tension loading, but the energy per unit area is essentially the same, indicating that the unit damage surface energy consumption is a fixed value when the specimen breaks. The strength of the concrete specimen under different loading conditions is caused by different stress states. Different conditions lead to different places within the cement where cracks begin to form and different directions for crack development. Macroscopic observation shows that the damage area is also different. Although the energy required per area for the formation of cracks is essentially the same, the energy required to form cracks over a larger area is greater. The greater the energy stored in the material, the greater the energy released when the specimen fails and the greater the strength of the specimen.

Figure 18: The failure of the specimen under dynamic tension loading.

Table 1: The damage area and damage energy for samples subjected to static pressure and static tension.

Loading method	Strength P (MPa)	Damage energy per unit area $\Delta\mu$ (MJ/cm^2)	Damage area S (m^2)	Damage energy U (J)
Static tension	3.5	1.12	0.005652	0.6342
Static pressure	35.5	1.21	0.320838	41

Using the method of Liang [15] were calculated the failure area and damage energy of concrete specimens under dynamic pressure and dynamic tension loading. Table 2 shows the results.

Tables 1 and 2 show that the damage strength of concrete is the largest for specimens subjected to dynamic pressure, followed closely by the strength of specimens under static pressure. The damage strength is much less for specimens subjected to static and dynamic tensile loading. The damage area is largest for dynamic pressure loading, followed by static pressure loading. The damage area of dynamic and static tensile loading is essentially the same. The damage energies produced by the fracture surface per unit area for the dynamic tension and dynamic pressure loading are essentially the same, and they are larger than for static loads. This is mainly because under dynamic loading, the cracks form throughout the aggregate, leading to greater strength, which requires more energy for cracks to form.

The stress states of the concrete specimens under dynamic pressure or the dynamic tension loading are different. Therefore, the degree of damage is different, the areas of crack formation are different, and the total energies required to form cracks are also different, resulting in different overall strengths. Different stress states are the root cause of the difference between the dynamic pressure strength and dynamic tensile strength.

We found that the destruction mechanisms of concrete under static and dynamic loadings are different. The development of mesoscopic cracks is faster for dynamic loading, the damage area is greater, and the increase in the number of crack points following energy release is greater. The microcracks cross the aggregate. In the static pressure loading tests, cracks have enough time to form along the weakest directions in the structure. Destruction due to static pressure and dynamic pressure leads to similar damage failure patterns. This is reflected in similar changes in CT numbers with increased loading. Both static and dynamic pressure loadings lead to initial increases in CT numbers followed by decreases. The static tensile crack development is distributed around the aggregate. It does not pass through the aggregate, making the fracture surface uneven. Dynamic stretching happens too quickly to find areas of weakness, so cracks will develop across the aggregate, resulting in fracture surfaces that are relatively flat.

Table 2: The damage area and damage energy for samples subjected to dynamic pressure and dynamic tensile loading.

Loading method	Strength P (MPa)	Damage energy per unit area $\Delta\mu$ (MJ/cm^2)	Damage area S (m^2)	Damage energy U (J)
Dynamic tensile	4.1	1.37	0.005652	0.7743
Dynamic pressure	37	1.32	0.426854	56

4. Conclusions

For a long time, the study of the mechanical properties of concrete has been based on macromechanics test methods. In this paper, we show how X-ray CT technology can be used to explore the failure process of concrete under pressure and tensile loading. The results showed the following:

(1) Under the dynamic loading, energy is released very quickly when concrete is damaged. Because the energy is released so quickly, it does not have time to find the weakest parts of the material to dissipate and form microcracks along these weak points. This results in microcracks along straight lines through the aggregate. A larger area of aggregate appears to break. This is why the dynamic strength is higher than the static strength of concrete.

(2) For dynamic pressure loading, there are more crack starting points, and the damage area is large. The damage is caused by the combination of many cracks. The damage for concrete under tensile loading is produced by a main crack through the specimen. The specimens under tension loading broke into two pieces, the concrete surfaces were smooth, and the cracks on the surfaces were small. This is why the concrete compressive strength is greater than the tensile strength.

(3) The energies for the formation of surface cracks per unit area for pressure loading and tension loading are essentially the same. The energy for the formation of surface cracks per unit area for dynamic loading is slightly more than for static loading.

Data Availability

The data used to support the findings of this study are available from the corresponding author upon request.

Conflicts of Interest

The authors declare that they have no conflicts of interest.

Acknowledgments

The study was supported by the Shaanxi Key Science and Technology Innovation Team (2016KCT-23).

References

[1] V. T. Giner, S. Ivorra, F. J. Baeza, and B. Ferrer, "Silica fume admixture effect on the dynamic properties of concrete," *Construction and Building Materials*, vol. 25, no. 8, pp. 3272–3277, 2011.

[2] X. D. Chen, S. X. Wu, and J. K. Zhou, "Experimental and modeling study of dynamic mechanical properties of cement paste,mortar and concrete," *Construction and Building Materials*, vol. 47, pp. 419–430, 2013.

[3] N. Selyutina and Y. Petrov, "The dynamic strength of concrete and macroscopic temporal parameter characterized in fracture process," *Procedia Structural Integrity*, vol. 2, pp. 438–445, 2016.

[4] J. Mazars and S. Grange, "Simplified strategies based on damage mechanics for concrete under dynamic loading," *Philosophical Transactions of the Royal Society*

A-Mathematical Physical and Engineering Sciences, vol. 375, no. 2085, article 20160170, 2017.

[5] H. M. Zelelew, A. Almuntashri, S. Agaian, and A. T. Papagiannakis, "An improved image processing technique for asphalt concrete X-ray CT images," *Road Materials and Pavement Design*, vol. 14, no. 2, pp. 341–359, 2013.

[6] M. Henry, I. S. Darma, and T. Sugiyama, "Analysis of effect of heating and re-curing on the microstructure of high-strength concrete using X-ray CT," *Construction and Building Materials*, vol. 67, pp. 37–46, 2014.

[7] H. Wang, Z. Huang, L. Li, Z. You, and Y. Chen, "Three-dimensional modeling and simulation of asphalt concrete mixtures based on X-ray CT microstructure images," *Journal of Traffic and Transportation Engineering*, vol. 1, no. 1, pp. 55–61, 2014.

[8] Y. Obara, I. Tanikura, J. Jung, R. Shintani, and S. Watanabe, "Evaluation of micro-damage of concrete specimens under cyclic uniaxial loading by X-ray CT method," *Journal of Advanced Concrete Technology*, vol. 14, no. 8, pp. 433–443, 2016.

[9] J. M. Raphael, "Tensile strength of concrete," *ACI Journal*, vol. 81, no. 2, pp. 158–165, 1984.

[10] W. D. Harris, E. C. Mohorovic, and T. P. Dolen, "Dynamic properties of mass concrete obtained from dam cores," *ACI Material Journal*, vol. 97, no. 3, pp. 290–296, 2000.

[11] E. Cadoni, G. Solomos, and C. Albertini, "Concrete behaviour in direct tension tests at high strain rates," *Magazine of Concrete Research*, vol. 65, no. 11, pp. 660–672, 2013.

[12] W. Elmer, E. Taciroglu, and L. McMichael, "Dynamic strength increase of plain concrete from high strain rate plasticity with shear dilation," *International Journal of Impact Engineering*, vol. 45, pp. 1–15, 2012.

[13] H. Chen and W. Ding, "Real time observation on meso fracture process of concrete using X-ray CT under uniaxial compressive condition," *Journal of Hydraulic Engineering*, vol. 37, no. 9, pp. 1044–1050, 2006.

[14] F. Dang, Y. Liu, W. Ding et al., "Quantitative analysis of concrete CT images based on damage fracture evolution theory," *Chinese Journal of Rock Mechanics and Engineering*, vol. 26, no. 8, pp. 1588–1594, 2007.

[15] X. Liang, *Concrete Intensity Mesomechanics Study Based on the Minimum Energy Principle*, Xi'An University of Technology, Xi'an, China, 2012.